Please cite this article in press as: Kural et al., Dynamics of Intracellular Clathrin/AP1- and Clathrin/AP3-Containing Carriers, Cell Reports (2012), http://dx.doi.org/10.1016/j.celrep.2012.09.025

Cell Reports
Report

Cell PRESS
Open ACCESS

Dynamics of Intracellular Clathrin/AP1- and Clathrin/AP3-Containing Carriers

Comert Kural,[1,3] Silvia K. Tacheva-Grigorova,[1] Steeve Boulant,[1,4] Emanuele Cocucci,[1] Thorsten Baust,[1,5] Delfim Duarte,[1,2] and Tom Kirchhausen[1,*]
[1]Department of Cell Biology, Harvard Medical School, Boston and Program in Cellular and Molecular Medicine at Boston Children's Hospital, Boston, MA 02115, USA
[2]Department of Biochemistry (U38), Faculty of Medicine, University of Porto, 4200-319 Porto, Portugal
[3]Present address: Department of Physics, Ohio State University, Columbus, OH 43210, USA
[4]Present address: Laboratory of Viral Infection and Innate Immune Sensing Dynamics, CHS Nachwuchsgruppe am CellNetworks Cluster und DKFZ, Heidelberg, Germany
[5]Present address: Boehringer Ingelheim RCV GmbH & Co KG, A-1121 Vienna, Austria
*Correspondence: kirchhausen@crystal.harvard.edu
http://dx.doi.org/10.1016/j.celrep.2012.09.025

SUMMARY

Clathrin/AP1- and clathrin/AP3-coated vesicular carriers originate from endosomes and the trans-Golgi network. Here, we report the real-time visualization of these structures in living cells reliably tracked by rapid, three-dimensional imaging with the use of a spinning-disk confocal microscope. We imaged relatively sparse, diffraction-limited, fluorescent objects containing chimeric fluorescent protein (clathrin light chain, σ adaptor subunits, or dynamin2) with a spatial precision of up to ~30 nm and a temporal resolution of ~1 s. The dynamic characteristics of the intracellular clathrin/AP1 and clathrin/AP3 carriers are similar to those of endocytic clathrin/AP2 pits and vesicles; the clathrin/AP1 coats are, on average, slightly shorter-lived than their AP2 and AP3 counterparts. We confirmed that although dynamin2 is recruited as a burst to clathrin/AP2 pits immediately before their budding from the plasma membrane, we found no evidence supporting a similar association of dynamin2 with clathrin/AP1 or clathrin/AP3 carriers at any stage during their lifetime. We found no effects of chemical inhibitors of dynamin function or the K44A dominant-negative mutant of dynamin on AP1 and AP3 dynamics. This observation suggests that an alternative budding mechanism, yet to be discovered, is responsible for the scission step of clathrin/AP1 and clathrin/AP3 carriers.

INTRODUCTION

Clathrin-based carriers are responsible for a large fraction of the endocytic traffic between the plasma membrane and endosomes, for traffic between endosomes, and for traffic between endosomes and the trans-Golgi network (TGN). Protein components of the clathrin coat selectively recruit cargo into the carrier. Assembly of the coat drives membrane engulfment into a clathrin-coated pit, which pinches off as a coated vesicle. Clathrin-coated pits and vesicles are diffraction-limited objects with typical diameters ranging between 75 and 130 nm. The smaller ~75 nm coats contain at least 36 copies of clathrin, a heterohexameric protein of three heavy chains and three light chains, and about half that number of copies of the heterotetrameric AP adaptor complex (Kirchhausen, 2000); the larger coats, which are more abundant, contain proportionally more clathrin and APs. Intracellular clathrin-coated vesicles contain AP1 or AP3 adaptors; endocytic clathrin-coated vesicles contain AP2 (Kirchhausen, 1999; Robinson and Bonifacino, 2001). The assembly of the endocytic clathrin-based carriers can be followed by expression of clathrin light chains or the σ2 subunit of AP2 fused with enhanced green fluorescent protein (EGFP) or related fluorescent proteins; suitably designed chimeric proteins do not affect the functional properties of the labeled carriers (Ehrlich et al., 2004). Thus, the dynamics of AP2-containing clathrin-coated structures at the surface of a cell attached to a glass coverslip have been studied by two-dimensional (2D) time-lapse imaging, using confocal or total internal reflection fluorescence microscopy (Cocucci et al., 2012; Ehrlich et al., 2004; Merrifield et al., 2005; Mettlen et al., 2009; Saffarian et al., 2009; Taylor et al., 2011; Yarar et al., 2005). Results from these experiments have shown that clathrin and AP2 adaptors are recruited continuously during coat formation and that the average lifetime of endocytic coats is 40–60 s.

Efforts to follow AP1-containing intracellular carriers have been less successful (Waguri et al., 2003), however, because the rapid three-dimensional (3D) movement of endosomes has not permitted one to distinguish initiation of assembly or dissociation of their coat from passage into or out of the imaging plane. No data are available for AP3. We have circumvented these problems by using a 3D tracking method that yields accurate results for relatively weak fluorescent objects that vary in position and intensity from image to image. The approach, which is simple to apply, uses data from 3D time series recorded with a spinning-disk confocal microscope from cells stably expressing σ1-EGFP or σ3-EGFP. It reveals previously undetected

properties of AP1- and AP3-containing carriers in mammalian cells. We find conclusive evidence for colocalization of AP-3 and clathrin in intracellular carriers. We also find that intracellular, AP-1-containing clathrin carriers are on average slightly shorter-lived than intracellular clathrin/AP3 and endocytic clathrin/AP2 carriers. The large GTPase, dynamin, drives the final pinching-off of a clathrin-coated membrane vesicle from a fully constricted coated pit (Hinshaw, 2000; Macia et al., 2006; Mettlen et al., 2009; Praefcke and McMahon, 2004; Sever et al., 2000; Urrutia et al., 1997). At the plasma membrane, this step requires acute recruitment of dynamin immediately following completion of clathrin/AP2 coat assembly (Ehrlich et al., 2004; Merrifield et al., 2002; Taylor et al., 2011), detected as a burst of fluorescence from dynamin2-EGFP just after the fluorescence from tagged clathrin has reached its maximum (Ehrlich et al., 2004; Lee et al., 2006; Massol et al., 2006; Taylor et al., 2011). Dynamin activity is also necessary at an earlier stage in endocytic-coated pit assembly: blocking dynamin with the small-molecule inhibitor, Dynasore (Kirchhausen et al., 2008; Macia et al., 2006), arrests clathrin incorporation before the coat has fully closed, but generally after at least half the clathrin has already accumulated (Macia et al., 2006), a result confirmed by measurements of the effect of overexpressed mutant dynamin on the maturation of endocytic clathrin-coated pits (Loerke et al., 2009). This assembly-arrest function appears to correspond to a steady recruitment of dynamin, at a level generally well below that of the fission-inducing burst, during the growth of an endocytic clathrin coat (Macia et al., 2006; Taylor et al., 2011).

We have examined the dynamics of dynamin recruitment and the effects of dynamin inhibition on the AP1- and AP3-containing clathrin carriers we can now detect. We find no evidence of a detectable burst of dynamin2-EGFP associated with clathrin/AP1 or clathrin/AP3 carriers at any point in their assembly-disassembly cycle, and we confirm this result by immunofluorescence imaging of endogenous dynamin2. In the same cells, dynamin2-EGFP exhibits the characteristic recruitment burst at clathrin/AP2-coated pits at the plasma membrane. Moreover, we find no evidence that treating cells with dynasore (3-hydroxy-naphthalene-2-carboxylic acid (3,4-dihydroxy-benzylidene)-hydrazide) or with its more active hydroxylated analog, dynasore-OH (3-hydroxy-*N*′-[(2,4,5-trihydroxyphenyl)methylidene]naphthalene-2-carbohydrazide) or dyngo-4a (Harper et al., 2011; Nguyen et al., 2012), prevents release of AP1- or AP3-containing carriers from the their donor membranes. These results are in line with the absence of effects from overexpressed dominant negative mutant dynamin K44A on the maturation of AP1- and AP3-containing carriers. These observations, which are also consistent with earlier work that demonstrated lack of functional interference with traffic along the secretory pathway by overexpression of dominant negative mutant dynamins, suggest that an alternative budding mechanism, yet to be discovered, is responsible for the scission step of clathrin/AP1 and clathrin/AP3 carriers.

RESULTS AND DISCUSSION

3D Tracking

We implemented a method for tracking the 3D position of a diffraction limited object with up to ~30 nm precision and for determining the fluorescence intensity associated with its 3D point-spread function. The approach is suitable for 3D time series recorded from living cells with a spinning-disk confocal microscope. It yields accurate results for relatively weak fluorescent objects that might vary in intensity from image to image.

Our tracking routine accepts data as a time series of z stacks, each plane in the stack being a recorded optical section. The required z spacing is approximately one-fourth to one-third of the full height of the point spread function (PSF); in the examples described here, $\Delta z \sim 250$–450 nm. We detect single fluorescent spots in the maximum projection image of a stack by a three-step procedure: 2D Gaussian and Laplacian filtering, followed by a local maximum-finding algorithm. The x and y positions of the spots are then obtained in a window of 7 × 7 pixels (94 nm per pixel) by a previously described 2D Gaussian fitting algorithm (Yildiz et al., 2003). For each spot, the 7 × 7 pixel window is then extended to each plane in the z stack, and integrated intensities for each plane are calculated by summing the pixel values and subtracting the local background. The background on each plane was determined in an 11 × 11 pixel window around each spot, by taking the average of the lowest-intensity pixel in each row. This average of minima ensures that no signal from a neighboring spot contributes to the calculation. The centroid of the intensity distribution in z was calculated as $C_z = \sum_{i=1}^{n} z_i I_i / \sum_{i=1}^{n} I_i$ where n is the number of planes in the z stack, z_i is the coordinate of a plane on the z axis, and I_i is the integrated signal of that plane. The integrated intensity of the plane with the minimum signal is the threshold subtracted from all planes.

To establish the feasibility of the localization method just described, we imaged AP1 adaptors tagged by stable expression in BSC1 cells of the small AP1 subunit, σ1, fused to EGFP (Figure 1A), rather than beads or other idealized objects. We first tested axial localization accuracy in fixed cells for AP1-carriers (Figure 1B) containing 20–40 EGFP fluorophores per spot (Figure S1) imaged in a spinning disk confocal microscope equipped with a piezo-driven stage. For a particular position of the stage, we recorded a set of ten independent z stacks (each stack containing seven optical sections at a spacing of 350 nm; Figure 1B). We then displaced the stage (and hence the cell) by 100 nm and recorded a second set of z stacks. We repeated the displacement three more times, yielding ten seven-plane z stacks for each of five stage positions. We determined, by the method outlined above, the z coordinate for the object in each of the ten stacks at different stage positions. The 100 nm steps taken by the stage were resolved with an estimated error of ~30 nm (Figure 1B) despite the relatively coarse sampling (the interval between optical sections was 350 nm and the total height of the point-spread function was nearly 1 μm); similar values were obtained using data from four instead of seven optical sections (red and green tracings, Figure 1B). Because the xy translations of our stage were not accurate enough to calibrate the precision by direct translation, we used instead the SD of the centroid determination in x and y, which were <10 nm, to set an accuracy of ~10 nm.

We then tested the applicability of the 3D approach in living cells by following the dynamics of an AP1-containing carrier in BSC1 cells. We recorded z stacks of five optical planes

Please cite this article in press as: Kural et al., Dynamics of Intracellular Clathrin/AP1- and Clathrin/AP3-Containing Carriers, Cell Reports (2012), http://dx.doi.org/10.1016/j.celrep.2012.09.025

Cell PRESS
Open ACCESS

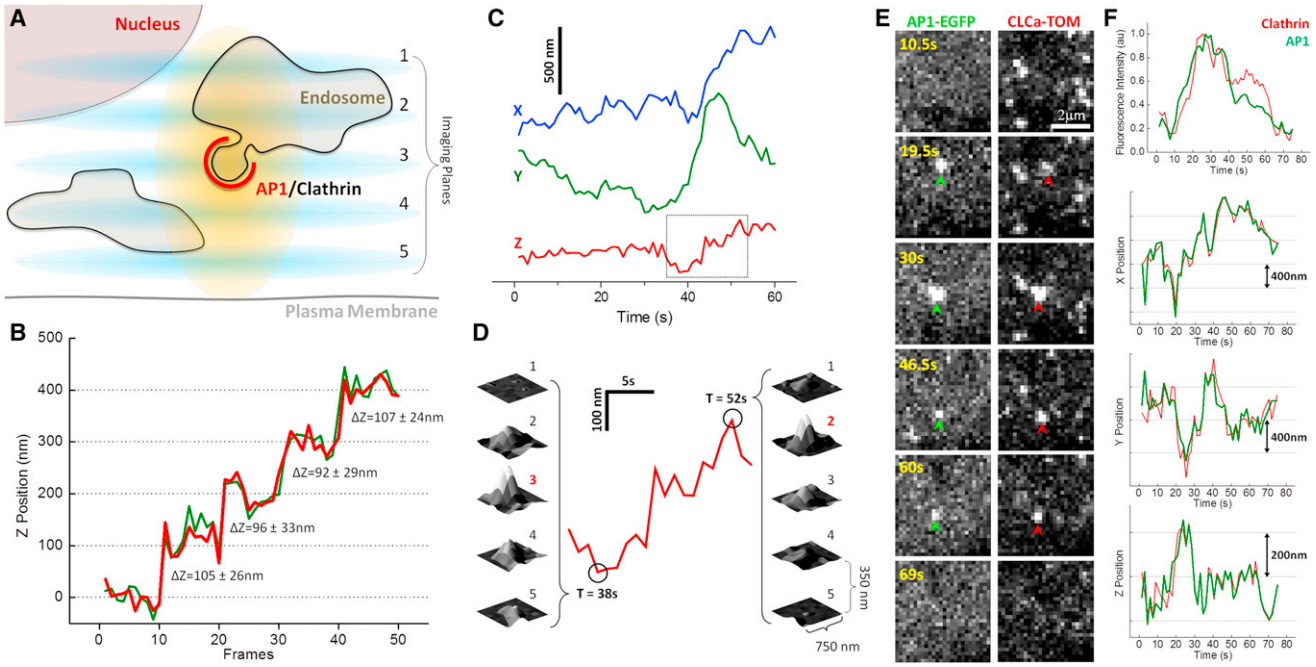

Figure 1. 3D Fluorescence Microscopy Visualization Strategy and Tracking

(A) Schematic representation of the 3D visualization strategy used to image the intracellular region of a cell.

(B) Determination of the axial accuracy of the 3D tracking procedure. The accuracy along the z axis was determined by imaging a single intracellular AP1 diffraction limited fluorescent spot from a chemically fixed BSC1 cell stably expressing σ1-EGFP. The spot was visualized by positioning the sample to different z positions spaced 100 nm apart, and then acquiring ten consecutive frames each composed of a z stack made of seven sequential optical sections separated by 350 nm obtained with 50 ms exposures. The same position of the fluorescence spot along the z axis was obtained by calculating the center of fluorescence intensity from four (green) or seven (red) sequential planes. Numeric values indicate step size measurement and estimated error using seven planes (see Experimental Procedures).

(C) Real-time 3D tracking of the relative x, y, and z displacements of a single diffraction limited AP1 spot visualized in a live BSC1 cell stably expressing σ1-EGFP. Data set obtained from a 60 s time series made of z stacks obtained every 1 s, each composed of five sequential images acquired with 25 ms exposures and spaced 350 nm apart.

(D) Expanded region of the z trace highlighted in (C). The surface representations correspond to the 2D fluorescence intensities of the spot from each of the contiguous planes acquired at 38 s and 52 s.

(E) Real-time tracking of a single fluorescent object containing AP1 (green arrow head) and clathrin (red arrow head) from a BSC1 cell stably expressing σ1-EGFP and transiently expressing clathrin LCa-Tomato. The images were simultaneously obtained on both fluorescent emission channels using a Dual View device placed in front of the camera and represent maximum intensity projections from z stacks obtained every 1.5 s each consisting of four planes acquired with 20 ms exposures and spaced 350 nm.

(F) Time dependence of the fluorescence intensity and displacements along the x, y, and z axis for the spot tracked in (E).

See also Figures S1, S2, and S4.

separated by 350 nm (after correction by the axial distortion); the time interval between stacks was 1 s; each exposure was for 25 ms. The x and y positions (Figure 1C) of a diffraction-limited, AP1-containing object followed for 60 s were determined at each time point from the center of a Gaussian fit to the maximum projected image of the stack. The corresponding z position, equivalent to the center of the intensity profile along the z axis, was established by centroid analysis of the integrated intensity of the spot determined in each plane (Figures 1C and 1D).

3D Tracking of AP1 and AP3 Clathrin-Coated Carriers

We proceeded to image a large number of intracellular AP1- or AP3-containing carriers (tagged by stable expression of σ1-EGFP or σ3-EGFP, respectively) in a volume defined by a region ~1–2 μm thick between the dorsal and ventral plasma membrane at the cell periphery or between the ventral surface and the nucleus immediately above it. By using this spatial constraint, we ensured that the carriers were completely tracked during the assembly and disassembly cycle of the coat. Acquisition of interpretable 3D tracings from the perinuclear region containing the TGN was not feasible, however, because the AP1 or AP3 fluorescent spots were so dense that single carriers were not resolvable. This imaging approach overcomes a significant limitation of 2D visualization with wide-field or single-plane laser confocal microscopy, in which movement of the carriers along the z axis leads to the possibility that appearance or disappearance of the fluorescence signal might be explained by entering or departing the imaging volume, rather than by initiation or dissociation of the coat.

We confirmed that all fluorescently tagged AP1- and AP3-containing structures were within the endosomal and perinuclear

Please cite this article in press as: Kural et al., Dynamics of Intracellular Clathrin/AP1- and Clathrin/AP3-Containing Carriers, Cell Reports (2012), http://dx.doi.org/10.1016/j.celrep.2012.09.025

Cell PRESS
Open ACCESS

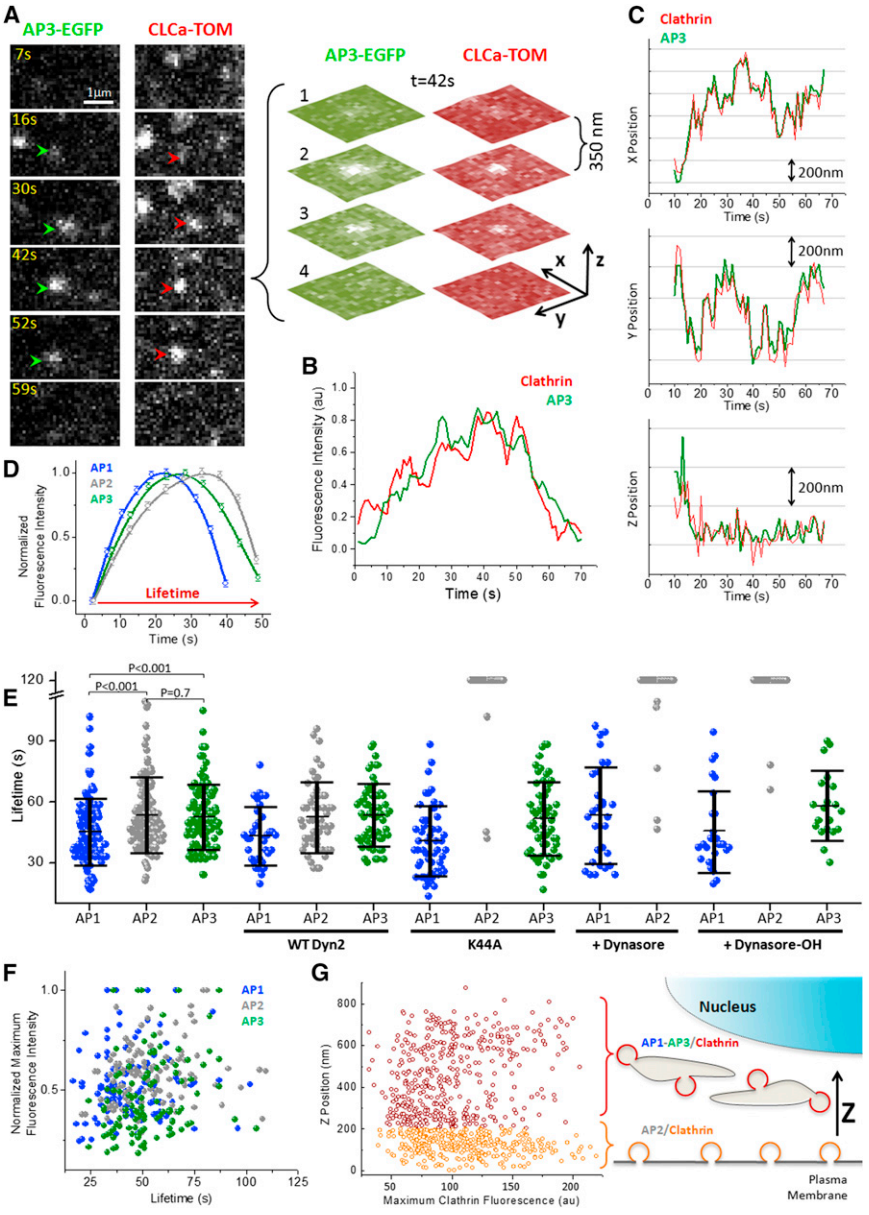

Figure 2. 3D Live Cell Imaging of Intracellular Clathrin Carriers in Living Cells

(A) Real-time tracking of a single fluorescent object containing AP3 and clathrin from a BSC1 cell stably expressing σ3-EGFP and transiently expressing clathrin LCa-Tomato. The images were simultaneously obtained on both fluorescent emission channels using a Dual View device placed in front of the camera and represent maximum intensity projections from z stacks obtained every 1 s each consisting of four planes acquired with 50 ms exposures and spaced 350 nm. The z stack obtained at 42 s is shown.

(B and C) Time dependence of the fluorescence intensity (B) and displacements along the x, y, and z axis (C) for the AP3/clathrin spot tracked in (A).

(D) Time dependence of the average fluorescence intensity of sets of AP1-, AP2-, and AP3-containing spots obtained from different 3D time series. Each trace was normalized to the maximal fluorescence intensities and average lifetimes of the corresponding set; error bars represent SE of the mean fluorescence intensity from data acquired from cells stably expressing σ1-EGFP (n = 187, 21 cells), σ2-EGFP (n = 455, 4 cells), and σ3-EGFP (n = 184, 25 cells).

(E) Lifetimes of single fluorescent spots calculated from individual 3D time series of AP1-, AP2-, and AP3-containing carriers in the absence (AP1: 45 ± 16 s, n = 125, 4 cells; AP2: 53 ± 18 s, n = 113, 2 cells; AP3: 53 ± 15 s, n = 110, 5 cells) or presence of 160 μM Dynasore (AP1: 53 ± 23 s, n = 30, 3 cells; AP2: n = 39, 3 cells) or 20 μM Dynasore-OH (AP1: 46 ± 20 s, n = 27, 3 cells; AP2: n = 32, 3 cells; AP3: 58 ± 17 s, n = 20, 2 cells). Lifetimes were also calculated for cells expressing WT dynamin2 (AP1: 43 ± 14 s, n = 35, 3 cells; AP2: 53 ± 17 s, n = 52, 4 cells; AP3: 53 ± 15 s, n = 60, 5 cells) or dominant negative K44A dynamin2 (AP1: 41 ± 17 s, n = 35, 3 cells; AP2: n = 43, 4 cells; AP3: 52 ± 18 s, n = 56, 7 cells). Data also shows average ± SD and p values used to determine the significance of the statistical differences calculated using the Student's t test.

(F) Scatter plot as a function of lifetime of the maximum florescence signal of single fluorescent spots calculated from individual 3D time series of AP1- (n = 125, 4 cells), AP2- (n = 113, 2 cells), and AP3-containing carriers (n = 110, 5 cells). The fluorescence intensities were normalized to the largest value of each set.

(G) Scatter plot corresponding to the maximum fluorescence intensity of clathrin-containing spots as a function of their relative z positions calculated from individual 3D time series. Spots located within 200 nm of the plasma membrane (orange) corresponded to endocytic AP2-containing carriers with maximum fluorescence intensities of 113 ± 41 (n = 336); the remaining spots (crimson) identified in the same cell corresponded to intracellular AP1- and AP3-containing carriers with maximum fluorescence intensity of 100 ± 38 (n = 415).

See also Figures S2, S3, and S4.

regions, but not at the plasma membrane of the stably expressing BSC1 cells (Figure S2), in agreement with previous immunofluorescence localization studies of endogenous AP1 and AP3 of other cell types (Dell'Angelica et al., 1997; Seaman et al., 1996). In addition we confirmed that all AP1 spots colocalized with clathrin (one representative example shown in Figures 1E and 1F) and found that AP3 also colocalized with clathrin tagged by transient expression of its light chain LCa fused to tomato (Figures 2A–2C and S3). We also established by immunofluorescence that stable expression of σ3-EGFP did not affect the extent of colocalization between objects containing AP3 and clathrin identified with a newly available anti-δ adaptin antibody (Peden et al., 2004) and an antibody specific for clathrin light chain (Figures S4A and S4B). The nearly complete colocalization of all AP3 spots with clathrin resolves a long-standing controversy concerning the extent of their association. Limitations inherent in the binding properties of different antibodies for AP3 or purification efficiency of AP3-containing coated vesicles

led to the previous uncertainties (Borner et al., 2012; Dell'Angelica et al., 1997; Robinson and Bonifacino, 2001).

We then measured the lifetimes of intracellular AP1- and AP3-containing carriers and compared them with the lifetimes of endocytic AP2-containing carriers (Figures 2D–2F). The average ±SD values for AP1-, AP2-, and AP3-containing carriers were 45 ± 16 s, 53 ± 18 s, and 53 ± 15 s, respectively (Figure 2E).

Most clathrin- and AP2-containing carriers are within 200 nm of the plasma membrane (Saffarian and Kirchhausen, 2008) (Figure 2G), whereas the AP1- and AP3-containing carriers are further displaced toward the cell interior (Figures 1A and 2G). By applying this simple geometric categorization, we could differentiate endocytic from intracellular clathrin events occurring within the same cell (Figure 2G) and hence control for variation due to expression level or extent of replacement of endogenous light chains with ectopically expressed LCa-EGFP. We then compared the final sizes of the clathrin coats associated with AP1 and AP3 intracellular carriers with those of coats associated with AP2 (Figure 2F) using the maximum fluorescence intensity of the clathrin signal as a measure of size (Ehrlich et al., 2004; Saffarian et al., 2009). Both sets of carriers had similar distributions of maximum clathrin fluorescence intensities, indicating a similar range of sizes for AP1-, AP2-, and AP3-containing carriers. This conclusion agrees with previous measurements from electron microscopy of fixed samples (Kirchhausen, 2000). Assuming that the molar ratio of clathrin to AP2 or to AP1 in the coated vesicles of these cells is the same as in brain (~0.7:1) (Blondeau et al., 2004), we estimate that like AP2-coated vesicles, a typical clathrin intracellular carrier contains 30–80 AP1 or AP3 adaptors. This range is consistent with the maximum number of σ1-EGFP or σ3-EGFP molecules associated with a given fluorescent spot (Figure S1) after a correction by a factor of 2 if one assumes an ~50% replacement of the endogenous σ1 or σ3 subunit with the ectopically stably expressed subunits, a replacement value determined for σ2 in AP-2 in BSC1 cells stably expressing σ2-EGFP (Cocucci et al., 2012). A biochemical confirmation of this analysis by western blot analysis is currently not possible because appropriate antibodies specific for σ1 or σ3 are not available.

Absence of Detectable Bursts of Dynamin Recruited to Intracellular Clathrin/AP1- and Clathrin/AP3-Containing Carriers

Mammalian genomes encode three dynamins. Dynamin1 is brain-specific, dynamin2 is ubiquitously expressed, and dynamin3 is found in brain, lung, and testis (Urrutia et al., 1997). It is well established that dynamin mediates budding of endocytic AP2/clathrin-coated vesicles from the plasma membrane (Hinshaw, 2000; Macia et al., 2006; Mettlen et al., 2009; Praefcke and McMahon, 2004; Sever et al., 2000). In this process, dynamin drives the fission of the membrane neck connecting the invaginated pit to the plasma membrane, in a process that requires acute recruitment of dynamin (Ehrlich et al., 2004; Taylor et al., 2011) around the neck immediately after completion of the clathrin/AP2 coat and prior to its uncoating. Complete assembly of endocytic clathrin/AP2 pits also depends on the steady recruitment of smaller amounts of dynamin during growth of the coat, particularly during later stages of coat formation (Macia et al., 2006).

Although these properties of dynamin have been thoroughly characterized for endocyticAP2/clathrin-coated pits, the targeting of dynamin to intracellular AP1- and AP3/clathrin-containing carriers and its possible role in maturation of these carriers remains controversial. Some immunolocalization studies showed targeting of endogenous dynamin to the perinuclear region (Jones et al., 1998; Maier et al., 1996; van Dam and Stoorvogel, 2002), whereas other immunofluorescence studies failed to show any significant localization of endogenous dynamin with clathrin, AP1, or TGN markers in the endosome-enriched perinuclear region (Altschuler et al., 1998; Kasai et al., 1999; Yoon et al., 1998). Only when dynamin2 was overexpressed could it consistently be found in perinuclear regions, by immunofluorescence, by immunoelectron microscopy visualization (Cao et al., 1998; Damke et al., 1994; Jones et al., 1998; Liu et al., 2011; Nicoziani et al., 2000), or by live cell imaging (data not shown). Overexpression of dominant negative forms of dynamin have also been used to test its effects of the intracellular traffic in intact cells; some groups reported no detectable effects (Altschuler et al., 1998; Banting et al., 1998; Damke et al., 1994; Kasai et al., 1999) whereas others reported inhibition (Bonazzi et al., 2005; Cao et al., 2000, 2005; Jones et al., 1998; Lauvrak et al., 2004; Nicoziani et al., 2000; van Dam and Stoorvogel, 2002). A more recent report showed that simultaneous elimination of dynamin1 and dynamin2 by gene knockout or by siRNA depletion had no effect on the perinuclear intracellular distribution of AP1, but the effects on the assembly dynamics of clathrin/AP1 carriers were not determined (Ferguson et al., 2009).

To resolve the uncertainties arising from these various observations, we used immunofluorescence to establish the extent of association of endogenous dynamin2, visualized in BSC1 cells with an antibody specific for dynamin2, with AP1, AP2, or AP3 fluorescently labeled by stable expression of σ1, σ2, or σ3-EGFP (Figure 3). We confirmed that many AP2-containing structures contained dynamin2 (24 ± 4%; 1,915 AP2 spots, n = 5 cells), reflecting that the association of dynamin2 with endocytic clathrin/AP2 pits, at low levels during coat assembly, and as an acute burst immediately before coated pit budding (Ehrlich et al., 2004; Macia et al., 2006; Taylor et al., 2011). In contrast, only a very small fraction of the AP1 or AP3 fluorescent spots (4 ± 1% and 5 ± 2%; n = 1,639 AP1 spots, n = 5 cells and 871 AP3 spots, n = 4 cells, respectively) showed detectable presence of dynamin2.

It is possible that steric hindrance of the dynamin epitope might explain the low level of association of the dynamin antibody with clathrin/AP1- or clathrin/AP3-containing carriers. We ruled out this by live cell imaging experiments carried out with human SK-MEL-2 cells expressing dynamin2 alone (hDNM2EN) or clathrin light chain A and dynamin2 (hCLTAEN/DNM2EN) (Doyon et al., 2011) (Figure 4). We took advantage that in these recently developed cell lines, there is full replacement of the endogenous untagged dynamin2 with a dynamin2-EGFP chimera, constitutively expressed at the same level as the native protein (Doyon et al., 2011). Expression of this dynamin2-EGFP has no detectable functional consequences for the cells. The hCLTAEN/DNM2EN cells also expressed clathrin light chain

Please cite this article in press as: Kural et al., Dynamics of Intracellular Clathrin/AP1- and Clathrin/AP3-Containing Carriers, Cell Reports (2012), http://dx.doi.org/10.1016/j.celrep.2012.09.025

Cell PRESS
Open ACCESS

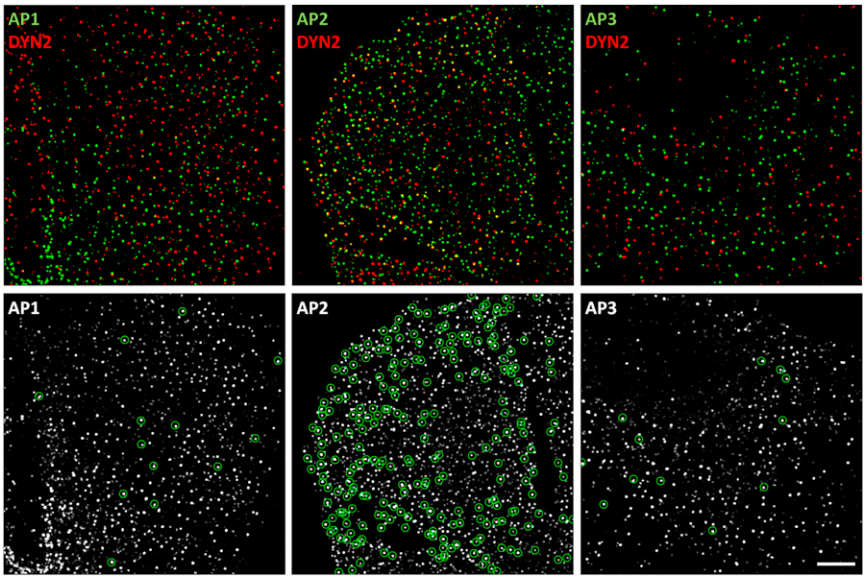

Figure 3. Extent of Colocalization of AP1, AP2, or AP3 with Dynamin2

Immunofluorescence of dynamin2 together with EGFP fluorescence imaging of AP1-, AP2-, and AP3-containing carriers in BSC1 cells stably expressing σ1-EGFP, σ2-EGFP, or σ3-EGFP visualized in 3D. The fixed samples were stained with an antibody specific for dynamin2 and imaged in 3D using optical sections spaced 0.1 μm. The views show maximum intensity z projections of images restored by constrained iterative deconvolution. The green circles (bottom panels) show instances of AP-carriers containing dynamin2. Scale bar represents 10 μm.

LCa-cherry, which replaced untagged endogenous LCa. We used live-cell, 3D imaging to compare in the same hCLTAEN/DNM2EN cells the recruitment of dynamin2 to the plasma membrane (e.g., to endocytic AP2/clathrin-containing structures) with the recruitment of dynamin2 to internal membranes including all intracellular, clathrin-containing structures (e.g., those containing AP1 or AP3). We collected time series in a volume ~1.8 μm thick, starting at the ventral plasma membrane and extending through the intracellular region to the dorsal (Figures 4A–4C). We confirmed that the 3D imaging approach correctly monitored the behavior of dynamin2-EGFP by demonstrating that most of the dynamin2-EGFP fluorescence diffraction-limited spots at the plasma membrane appeared as transient events with rapid kinetics. As expected, the majority of these spots (~80%) colocalized with LCa-cherry, displaying the characteristic burst of dynamin recruitment toward the end of the clathrin growth phase and immediately before the clathrin uncoating step (Figure 4C). Similar dynamin2-EGFP kinetics were observed at the plasma membrane of hDNM2EN cells, in which dynamin2-EGFP is the only protein that has replaced its wild-type counterpart, indicating that the dynamin behavior is not influenced by expression of clathrin light chain LCa-cherry (not shown). In contrast to dynamin activity at the plasma membrane, we detected very few dynamin2-EGFP fluorescent spots in the intracellular region of the same two types of cells (Figures 4B and 4D); the few detected spots failed to display the rapid formation and disappearance that would report an acute recruitment to intracellular sites. These live cell-imaging results show that the budding mechanism of intracellular clathrin/AP1- and clathrin/AP3-containing carriers does not involve a process with dynamics that resemble the acute recruitment of dynamin2 to budding endocytic clathrin/AP2 carriers at the plasma membrane.

Our failure to detect dynamin associated with AP1- or AP3-containing carriers indicates that no more than a limited amount of dynamin is likely to associate with these structures. It does not rule out a potential parallel for the activity of dynamin that is required to avoid mid- to late-stage assembly arrest of endocytic-coated vesicles (Macia et al., 2006), because the associated accumulation could have been below the threshold of detection in our experiments. To test this possibility, we examined the effects of inhibiting dynamin on AP1 and AP3 dynamics, and found that adding 160 μM to cells expressing σ1- or σ3-EGFP had no detectable effect on the dynamics of AP1 and AP3 (Figure 2E). Moreover, addition of dynasore-OH, a more potent analog of dynasore, also had no detectable effect on AP1 and AP3 dynamics (20 μM dynasore-OH [Figure 2E] or 40 μM [not shown]). As a positive control for the inhibitory endocytic effect of dynasore or dynasore-OH, we established that transferrin uptake in the same cells was completely blocked (not shown), as were AP2 dynamics (Figure 2E). These experiments were complemented by examining AP dynamics in BSC1 cells following transient expression of WT dynamin2 or the dynamin2 mutant K44A 16 hr postviral transduction (Altschuler et al., 1998). Under these conditions, expression of the dynamin2 K44A mutant but not WT dynamin2 fully inhibited AP2 dynamics and strongly blocked receptor-mediated endocytosis of transferrin in every cell observed in the field (Figure 2E and data not shown). We found no evidence, however, of inhibition of AP1 and AP3 dynamics (Figure 2E) even though the uptake of transferrin was also blocked in cells expressing σ1- or σ3-EGFP (data not shown). These results are consistent with electron microscopy data showing accumulation of incomplete coated structures at the plasma membrane but not in the perinuclear region (Damke et al., 1994) and are in agreement with absence of defects in clathrin-dependent intracellular traffic in cells overexpressing dominant negative forms of dynamin (Altschuler et al., 1998; Banting et al., 1998; Damke et al., 1994; Kasai et al., 1999). These observations suggest that dynamin is not used for the scission of AP1 and AP3 carriers and that their budding may be different in mechanism from the budding of AP2-containing carriers.

We have noticed that expression of WT or mutant dynamin2 driven by viral transduction or plasmid transfection decreased the fluorescence intensity of all σ-EGFP subunits associated with APs spots, presumably a result of promoter competition. This effect is particularly strong 24 hr posttransfection, a period

Please cite this article in press as: Kural et al., Dynamics of Intracellular Clathrin/AP1- and Clathrin/AP3-Containing Carriers, Cell Reports (2012), http://dx.doi.org/10.1016/j.celrep.2012.09.025

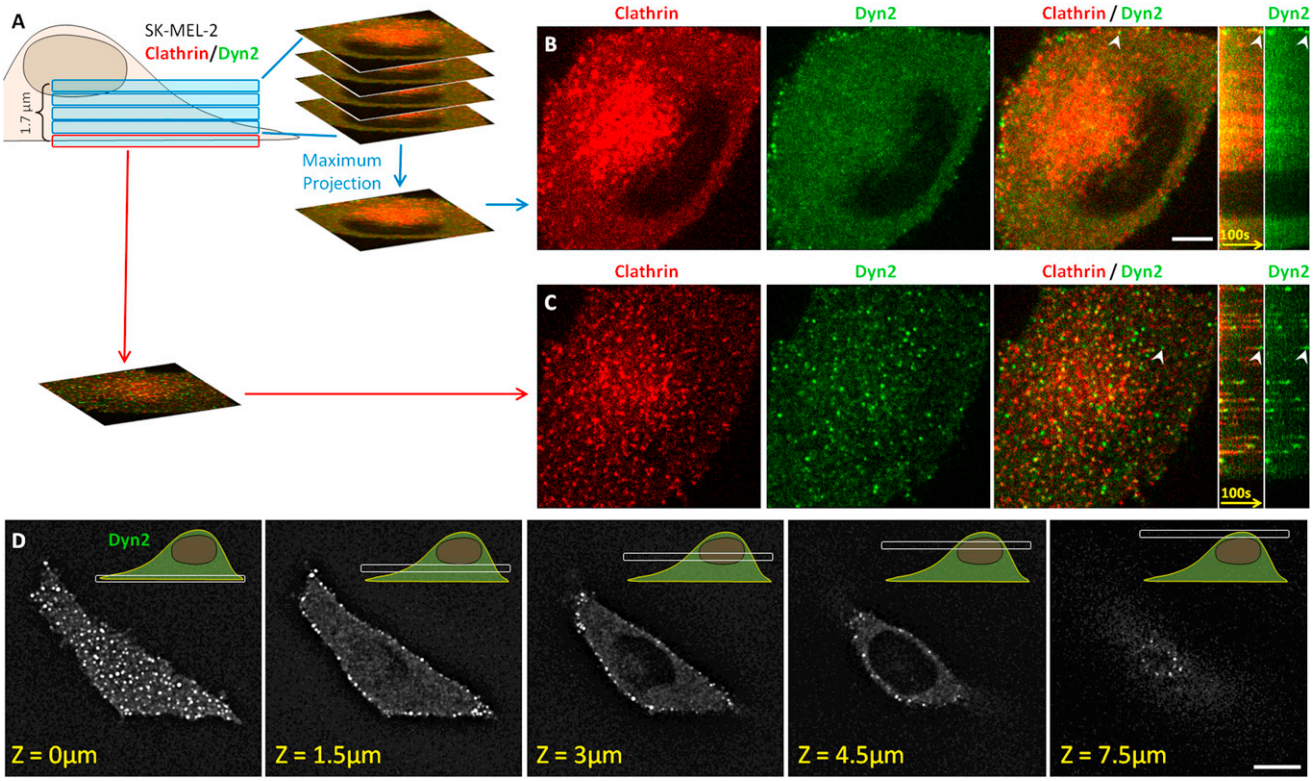

Figure 4. 3D Live Cell Imaging of Genome-Edited Cells Expressing Fluorescently Tagged Clathrin and Dynamin2

(A) Visualization strategy used to acquire the 3D time series shown at the right in (B) and (C) using SK-MEL-2 cells stably expressing clathrin light chain A and dynamin2 (hCLTAEN/DNM2EN). Each z stack consisted of five sequential optical sections spaced by 350 nm obtained every 2 s using 30 ms exposures.

(B) Snapshot from a maximum intensity projection and corresponding kymograph obtained from the top four optical sections corresponding to the intracellular region containing the TGN and endosomes (highlighted by the concentrated clathrin signal) showed absence of fluorescence bursts of dynamin2-EGFP. The bright dynamin2-EGFP at the cell periphery associated with endocytic clathrin LCa-RFP-containing carrier, an example of which is highlighted by the arrowhead. Scale bar represents 10 μm.

(C) Snapshot from the bottom optical section containing the plasma membrane and corresponding kymograph acquired from the same cell imaged in (B). It showed numerous fluorescence bursts of dynamin2-EGFP associated with clathrin LCa-RFP prior to clathrin coat disassembly; the arrowhead highlights a representative example.

(D) Selected optical sections obtained from a 3D live cell imaging series obtained from a SK-MEL-2 cell stably expressing dynamin2-EGFP (DNM2EN). The z stack consisted of 25 optical sections separated by 350 nm and imaged with 100 ms exposures. Bright dynamin2-EGFP were only observed at the cell periphery. Scale bar represents 10 μm.

required in order to block endocytosis due to the accumulation of sufficient amounts of dynaminK44A, so that it was not possible to detect fluorescent spots containing σ1, σ2, or σ3-EGFP, even though the localization of APs spots detected by immune fluorescence microscopy was not affected (not shown).

Conclusions

We have used data from 3D time series corresponding to z stacks recorded with a spinning-disk confocal microscope to follow the fate of AP1- and AP3-containing intracellular carriers. We have been able to track them from assembly to uncoating, despite their relatively rapid motion in all three dimensions. These structures have lifetimes and sizes (the latter as estimated from maximum fluorescence intensity) comparable to those of endocytic, clathrin-coated AP2/clathrin-containing carriers. We were unable to detect participation of dynamin in AP1- and AP3-directed clathrin carrier formation either during coat assembly or at the vesicular pinching off steps. The molecular mediators of membrane fission for these carriers remain to be determined.

EXPERIMENTAL PROCEDURES

Reagents, Cell Culture, and Transfections

Monkey BSC1 cells stably expressing σ2-EGFP (Ehrlich et al., 2004; Saffarian and Kirchhausen, 2008), σ1-EGFP (Anitei et al., 2010), or σ3a-EGFP and human SK-MEL-2 cells expressing dynamin2-EGFP (hDNM2EN) or clathrin light chain A fused to RFP and dynamin2-EGFP (hCLTAEN/DNM2EN) in their native genomic loci (Doyon et al., 2011) were grown in DMEM medium containing 10% fetal calf serum, penicillin, and streptomycin. Transient expression of 2 μg rat Tomato-LCa (Massol et al., 2006) in BSC1 cells was carried out using Lipofectamine 2000 (Invitrogen) in Optimem (GIBCO) according to the manufacturer's instructions and were analyzed 24 hr after transfection. Transient expression of WT and the K44A dominant negative mutant of dynamin2 were achieved by adenovirus transduction and cells analyzed for AP dynamics and fluorescence transferrin uptake 16 hr postinfection (Altschuler et al., 1998). The rabbit polyclonal anti-dynamin 2 (ab3457, Abcam, Cambridge, MA) antibody, mouse monoclonal anti-δ-adaptin antibody (Peden

et al., 2004) (anti-delta SA4, Developmental Studies Hybridoma Bank, Iowa City, IA), rabbit polyclonal anti-clathrin light chain antibody (kindly provided by F. Brodsky, UCSF, San Francisco, CA), and Alexa Fluor 647 goat anti-rabbit and Alexa Fluor 568 donkey anti-rabbit antibodies (Invitrogen, Grand Island, NY) were used for immunofluorescence.

Immunofluorescence

Approximately 4–6 × 10^4 BSC1 cells were plated on 18 mm in diameter No. 1.5 glass coverslips and allowed to grow for 24 hr at 37°C and 5% CO_2 in DMEM supplemented with 10% FCS. The cells were then washed three times with PBS at room temperature and fixed for 10 min with ice-cold 4% paraformaldehyde in PBS, pH 7.4, followed by three washes in PBS and two washes of 10 min each with 0.1 M glycine (Figure 2) or 50 mM ammonium chloride (Figure S4), and finally rinsed with PBS supplemented with 1% BSA. Cell were then incubated at room temperature for 1 hr with the antibody specific for dynamin 2 dissolved in PBS containing 1% BSA and 0.1% TX-100 (Figure 2) or for clathrin and δ3-adaptin dissolved in PBS containing 5% BSA and 0.1% TX-100 (Figure S4). The cells were washed five times with PBS and 1% or 5% BSA then incubated for 45 min at room temperature with secondary antibodies in PBS and 1% or 5% BSA. After several washes in PBS, the samples were mounted and imaged in 90% glycerol in PBS.

Live Cell Spinning Disk Confocal Imaging

Approximately 1 × 10^5 BSC1 or SK-MEL-2 cells were plated 16 hr prior to imaging on 25 mm in diameter No. 1.5 glass coverslips. Imaging medium was phenol red free DMEM supplemented with 10% FCS and 20 mM HEPES pH 7.4. For imaging, the coverslips were placed on a temperature-controlled 5% CO_2 humidified chamber (20/20 Technologies, Wilmington, NC) mounted on the piezo-electric driven stage of a Mariana imaging system (Intelligent Imaging Innovations, Denver, CO) based on an Axiovert 200M inverted microscope (Carl Zeiss, Thornwood, NY), a CSU-X1 spinning disk confocal unit (Yokogawa Electric, Tokyo, Japan), a spherical aberration correction device (SAC, Infinity Photo-Optical, Boulder, CO) and a 63× objective lens (Plan-Apochromat, NA 1.4, Carl Zeiss). The SAC was placed between the oil-based objective lens and the camera to resolve the spherical aberration introduced by the refractive index mismatch between living cells and the glass optics. The data acquired for the experiments using the SK-MEL-2 cells were obtained with a CSU-22 spinning disk confocal unit (Yokogawa Electric) modified with a Borealis illumination system (Spectral Applied Research, Richmond Hill, Ontario, Canada) and without SAC correction. Fluorescence images from cells expressing EGFP and RFP chimeras were simultaneously collected on two sides of the same CCD chip by using a dual view unit (Roper Scientific) mounted before the camera and equipped with a 565DCXR dichroic mirror and HQ525/40 and HQ620/50 (Chroma) emission filters (Saffarian et al., 2009). All the data were acquired using Slidebook 5 (Intelligent Imaging Innovations, Denver, CO).

Data Acquisition and Image Analysis

Three-dimensional time-lapse movies correspond to z stacks of four to six consecutive optical planes spaced 0.25–0.45 μm after correction by the axial distortion (equivalent to 0.36–0.64 μm displacement of the stage). Axial distortion (elongation) stemming from the refractive index mismatch between the glass coverslip and the biological sample was corrected by applying an axial correction value of 0.7 (Ferko et al., 2006; Lu et al., 2009) obtained by imaging 15 μm fluorescent polystyrene beads with the spinning disk confocal microscope equipped with the spherical aberration correction device. All z distances reported in the figures have been corrected by the axial distortion. The 3D data were acquired at a frequency of 0.3–2 Hz per stack and 20–50 ms exposures per frame; the movies had durations between 120 and 330 s. Slidebook 5 was used to generate a maximum intensity z projection from each time point of the 3D time series. Custom made MATLAB-based algorithms were used to determine the fluorescence intensity of a given diffraction limited spot and their location along the x and y axis (from the maximum intensity images) and along the z axis (from the z stacks). Step sizes for the data in Figure 1B were calculated as $\Delta z_i = \bar{z}_{i+1} - \bar{z}_i$, where $\bar{z}_i$ is the average position of step number *i*. The SD of Δz_i was calculated by error propagation: $\sigma^2_{\Delta z_i} = \sigma^2_{\bar{z}_{i+1}} + \sigma^2_{\bar{z}_i}$.

The colocalization analysis of APs with dynamin2 was performed using fixed BSC1 cells imaged with the spinning disk confocal microscope. Three-dimensional images made of z stacks composed of 0.1 μm sequential optical sections were restored using constrained iterative deconvolution (SlideBook 5). Three-dimensional binary masks were then created by segmentation for both fluorescence channels (APs and dynamin2), and overlapping regions were determined using the AND operator between the two masks. Each overlapping region was counted as a colocalization event.

SUPPLEMENTAL INFORMATION

Supplemental Information includes four figures and can be found with this article online at http://dx.doi.org/10.1016/j.celrep.2012.09.025.

LICENSING INFORMATION

This is an open-access article distributed under the terms of the Creative Commons Attribution 3.0 Unported License (CC-BY; http://creativecommons.org/licenses/by/3.0/legalcode).

ACKNOWLEDGMENTS

We thank Lei Lu for preparing the sample and the data used to generate Figure S1, Eric Marino for maintaining the Imaging Resource used in this study, Frances Brodsky for the clathrin light chain antibody, Marcel Mettlen and Sandy Schmid for the adenovirus encoding WT and dynamin2K44A and Pietro DeCamilli, Marc McNiven, Sandy Schmid and members of our laboratory for helpful discussions. Comert Kural is a recipient of a Helen Hay Whitney Foundation Fellowship. Delfim Duarte was supported by the Harvard Medical School-Portugal Program in Translational Research and Information and by a summer travel fellowship from the Fundação Luso-Americana para o Desenvolvimento (FLAD). This work was supported in part by NIH grant GM-075252 (T.K.) and U54 AI057159 (New England Regional Center of Excellence in Biodefense and Emerging Infectious Disease, Core Imaging Facility).

Received: December 16, 2011
Revised: June 5, 2012
Accepted: September 19, 2012
Published: October 25, 2012

REFERENCES

Altschuler, Y., Barbas, S.M., Terlecky, L.J., Tang, K., Hardy, S., Mostov, K.E., and Schmid, S.L. (1998). Redundant and distinct functions for dynamin-1 and dynamin-2 isoforms. J. Cell Biol. *143*, 1871–1881.

Anitei, M., Stange, C., Parshina, I., Baust, T., Schenck, A., Raposo, G., Kirchhausen, T., and Hoflack, B. (2010). Protein complexes containing CYFIP/Sra/PIR121 coordinate Arf1 and Rac1 signalling during clathrin-AP-1-coated carrier biogenesis at the TGN. Nat. Cell Biol. *12*, 330–340.

Banting, G., Maile, R., and Roquemore, E.P. (1998). The steady state distribution of humTGN46 is not significantly altered in cells defective in clathrin-mediated endocytosis. J. Cell Sci. *111*, 3451–3458.

Blondeau, F., Ritter, B., Allaire, P.D., Wasiak, S., Girard, M., Hussain, N.K., Angers, A., Legendre-Guillemin, V., Roy, L., Boismenu, D., et al. (2004). Tandem MS analysis of brain clathrin-coated vesicles reveals their critical involvement in synaptic vesicle recycling. Proc. Natl. Acad. Sci. USA *101*, 3833–3838.

Bonazzi, M., Spanò, S., Turacchio, G., Cericola, C., Valente, C., Colanzi, A., Kweon, H.S., Hsu, V.W., Polishchuck, E.V., Polishchuck, R.S., et al. (2005). CtBP3/BARS drives membrane fission in dynamin-independent transport pathways. Nat. Cell Biol. *7*, 570–580.

Borner, G.H.H., Antrobus, R., Hirst, J., Bhumbra, G.S., Kozik, P., Jackson, L.P., Sahlender, D.A., and Robinson, M.S. (2012). Multivariate proteomic profiling identifies novel accessory proteins of coated vesicles. J. Cell Biol. *197*, 141–160.

Cao, H., Garcia, F., and McNiven, M.A. (1998). Differential distribution of dynamin isoforms in mammalian cells. Mol. Biol. Cell *9*, 2595–2609.

Cao, H., Thompson, H.M., Krueger, E.W., and McNiven, M.A. (2000). Disruption of Golgi structure and function in mammalian cells expressing a mutant dynamin. J. Cell Sci. *113*, 1993–2002.

Cao, H., Weller, S., Orth, J.D., Chen, J., Huang, B., Chen, J.-L., Stamnes, M., and McNiven, M.A. (2005). Actin and Arf1-dependent recruitment of a cortactin-dynamin complex to the Golgi regulates post-Golgi transport. Nat. Cell Biol. *7*, 483–492.

Cocucci, E., Aguet, F., Boulant, S., and Kirchhausen, T. (2012). The first five seconds in the life of a clathrin-coated pit. Cell *150*, 495–507.

Damke, H., Baba, T., Warnock, D.E., and Schmid, S.L. (1994). Induction of mutant dynamin specifically blocks endocytic coated vesicle formation. J. Cell Biol. *127*, 915–934.

Dell'Angelica, E.C., Ohno, H., Ooi, C.E., Rabinovich, E., Roche, K.W., and Bonifacino, J.S. (1997). AP-3: an adaptor-like protein complex with ubiquitous expression. EMBO J. *16*, 917–928.

Doyon, J.B., Zeitler, B., Cheng, J., Cheng, A.T., Cherone, J.M., Santiago, Y., Lee, A.H., Vo, T.D., Doyon, Y., Miller, J.C., et al. (2011). Rapid and efficient clathrin-mediated endocytosis revealed in genome-edited mammalian cells. Nat. Cell Biol. *13*, 331–337.

Ehrlich, M., Boll, W., Van Oijen, A., Hariharan, R., Chandran, K., Nibert, M.L., and Kirchhausen, T. (2004). Endocytosis by random initiation and stabilization of clathrin-coated pits. Cell *118*, 591–605.

Ferguson, S.M., Raimondi, A., Paradise, S., Shen, H., Mesaki, K., Ferguson, A., Destaing, O., Ko, G., Takasaki, J., Cremona, O., et al. (2009). Coordinated actions of actin and BAR proteins upstream of dynamin at endocytic clathrin-coated pits. Dev. Cell *17*, 811–822.

Ferko, M.C., Patterson, B.W., and Butler, P.J. (2006). High-resolution solid modeling of biological samples imaged with 3D fluorescence microscopy. Microsc. Res. Tech. *69*, 648–655.

Harper, C.B., Martin, S., Nguyen, T.H., Daniels, S.J., Lavidis, N.A., Popoff, M.R., Hadzic, G., Mariana, A., Chau, N., McCluskey, A., et al. (2011). Dynamin inhibition blocks botulinum neurotoxin type A endocytosis in neurons and delays botulism. J. Biol. Chem. *286*, 35966–35976.

Hinshaw, J.E. (2000). Dynamin and its role in membrane fission. Annu. Rev. Cell Dev. Biol. *16*, 483–519.

Jones, S.M., Howell, K.E., Henley, J.R., Cao, H., and McNiven, M.A. (1998). Role of dynamin in the formation of transport vesicles from the trans-Golgi network. Science *279*, 573–577.

Kasai, K., Shin, H.W., Shinotsuka, C., Murakami, K., and Nakayama, K. (1999). Dynamin II is involved in endocytosis but not in the formation of transport vesicles from the trans-Golgi network. J. Biochem. *125*, 780–789.

Kirchhausen, T. (1999). Adaptors for clathrin-mediated traffic. Annu. Rev. Cell Dev. Biol. *15*, 705–732.

Kirchhausen, T. (2000). Clathrin. Annu. Rev. Biochem. *69*, 699–727.

Kirchhausen, T., Macia, E., and Pelish, H.E. (2008). Use of dynasore, the small molecule inhibitor of dynamin, in the regulation of endocytosis. Methods Enzymol. *438*, 77–93.

Lauvrak, S.U., Torgersen, M.L., and Sandvig, K. (2004). Efficient endosome-to-Golgi transport of Shiga toxin is dependent on dynamin and clathrin. J. Cell Sci. *117*, 2321–2331.

Lee, D.-W., Wu, X., Eisenberg, E., and Greene, L.E. (2006). Recruitment dynamics of GAK and auxilin to clathrin-coated pits during endocytosis. J. Cell Sci. *119*, 3502–3512.

Liu, Y.W., Lukiyanchuk, V., and Schmid, S.L. (2011). Common membrane trafficking defects of disease-associated dynamin 2 mutations. Traffic *12*, 1620–1633.

Loerke, D., Mettlen, M., Yarar, D., Jaqaman, K., Jaqaman, H., Danuser, G., and Schmid, S.L. (2009). Cargo and dynamin regulate clathrin-coated pit maturation. PLoS Biol. *7*, e57.

Lu, L., Ladinsky, M.S., and Kirchhausen, T. (2009). Cisternal organization of the endoplasmic reticulum during mitosis. Mol. Biol. Cell *20*, 3471–3480.

Macia, E., Ehrlich, M., Massol, R., Boucrot, E., Brunner, C., and Kirchhausen, T. (2006). Dynasore, a cell-permeable inhibitor of dynamin. Dev. Cell *10*, 839–850.

Maier, O., Knoblich, M., and Westermann, P. (1996). Dynamin II binds to the trans-Golgi network. Biochem. Biophys. Res. Commun. *223*, 229–233.

Massol, R.H., Boll, W., Griffin, A.M., and Kirchhausen, T. (2006). A burst of auxilin recruitment determines the onset of clathrin-coated vesicle uncoating. Proc. Natl. Acad. Sci. USA *103*, 10265–10270.

Merrifield, C.J., Feldman, M.E., Wan, L., and Almers, W. (2002). Imaging actin and dynamin recruitment during invagination of single clathrin-coated pits. Nat. Cell Biol. *4*, 691–698.

Merrifield, C.J., Perrais, D., and Zenisek, D. (2005). Coupling between clathrin-coated-pit invagination, cortactin recruitment, and membrane scission observed in live cells. Cell *121*, 593–606.

Mettlen, M., Pucadyil, T., Ramachandran, R., and Schmid, S.L. (2009). Dissecting dynamin's role in clathrin-mediated endocytosis. Biochem. Soc. Trans. *37*, 1022–1026.

Nguyen, T.H., Maucort, G., Sullivan, R.K.P., Schenning, M., Lavidis, N.A., McCluskey, A., Robinson, P.J., and Meunier, F.A. (2012). Actin- and dynamin-dependent maturation of bulk endocytosis restores neurotransmission following synaptic depletion. PLoS ONE *7*, e36913.

Nicoziani, P., Vilhardt, F., Llorente, A., Hilout, L., Courtoy, P.J., Sandvig, K., and van Deurs, B. (2000). Role for dynamin in late endosome dynamics and trafficking of the cation-independent mannose 6-phosphate receptor. Mol. Biol. Cell *11*, 481–495.

Peden, A.A., Oorschot, V., Hesser, B.A., Austin, C.D., Scheller, R.H., and Klumperman, J. (2004). Localization of the AP-3 adaptor complex defines a novel endosomal exit site for lysosomal membrane proteins. J. Cell Biol. *164*, 1065–1076.

Praefcke, G.J., and McMahon, H.T. (2004). The dynamin superfamily: universal membrane tubulation and fission molecules? Nat. Rev. Mol. Cell Biol. *5*, 133–147.

Robinson, M.S., and Bonifacino, J.S. (2001). Adaptor-related proteins. Curr. Opin. Cell Biol. *13*, 444–453.

Saffarian, S., and Kirchhausen, T. (2008). Differential evanescence nanometry: live-cell fluorescence measurements with 10-nm axial resolution on the plasma membrane. Biophys. J. *94*, 2333–2342.

Saffarian, S., Cocucci, E., and Kirchhausen, T. (2009). Distinct dynamics of endocytic clathrin-coated pits and coated plaques. PLoS Biol. *7*, e1000191.

Seaman, M.N.J., Sowerby, P.J., and Robinson, M.S. (1996). Cytosolic and membrane-associated proteins involved in the recruitment of AP-1 adaptors onto the trans-Golgi network. J. Biol. Chem. *271*, 25446–25451.

Sever, S., Damke, H., and Schmid, S.L. (2000). Garrotes, springs, ratchets, and whips: putting dynamin models to the test. Traffic *1*, 385–392.

Taylor, M.J., Perrais, D., and Merrifield, C.J. (2011). A high precision survey of the molecular dynamics of mammalian clathrin-mediated endocytosis. PLoS Biol. *9*, e1000604.

Urrutia, R., Henley, J.R., Cook, T., and McNiven, M.A. (1997). The dynamins: redundant or distinct functions for an expanding family of related GTPases? Proc. Natl. Acad. Sci. USA *94*, 377–384.

van Dam, E.M., and Stoorvogel, W. (2002). Dynamin-dependent transferrin receptor recycling by endosome-derived clathrin-coated vesicles. Mol. Biol. Cell *13*, 169–182.

Waguri, S., Dewitte, F., Le Borgne, R., Rouillé, Y., Uchiyama, Y., Dubremetz, J.-F., and Hoflack, B. (2003). Visualization of TGN to endosome trafficking through fluorescently labeled MPR and AP-1 in living cells. Mol. Biol. Cell *14*, 142–155.

Yarar, D., Waterman-Storer, C.M., and Schmid, S.L. (2005). A dynamic actin cytoskeleton functions at multiple stages of clathrin-mediated endocytosis. Mol. Biol. Cell *16*, 964–975.

Yildiz, A., Forkey, J.N., McKinney, S.A., Ha, T., Goldman, Y.E., and Selvin, P.R. (2003). Myosin V walks hand-over-hand: single fluorophore imaging with 1.5-nm localization. Science *300*, 2061–2065.

Yoon, Y., Pitts, K.R., Dahan, S., and McNiven, M.A. (1998). A novel dynamin-like protein associates with cytoplasmic vesicles and tubules of the endoplasmic reticulum in mammalian cells. J. Cell Biol. *140*, 779–793.

Cell PRESS
Open ACCESS

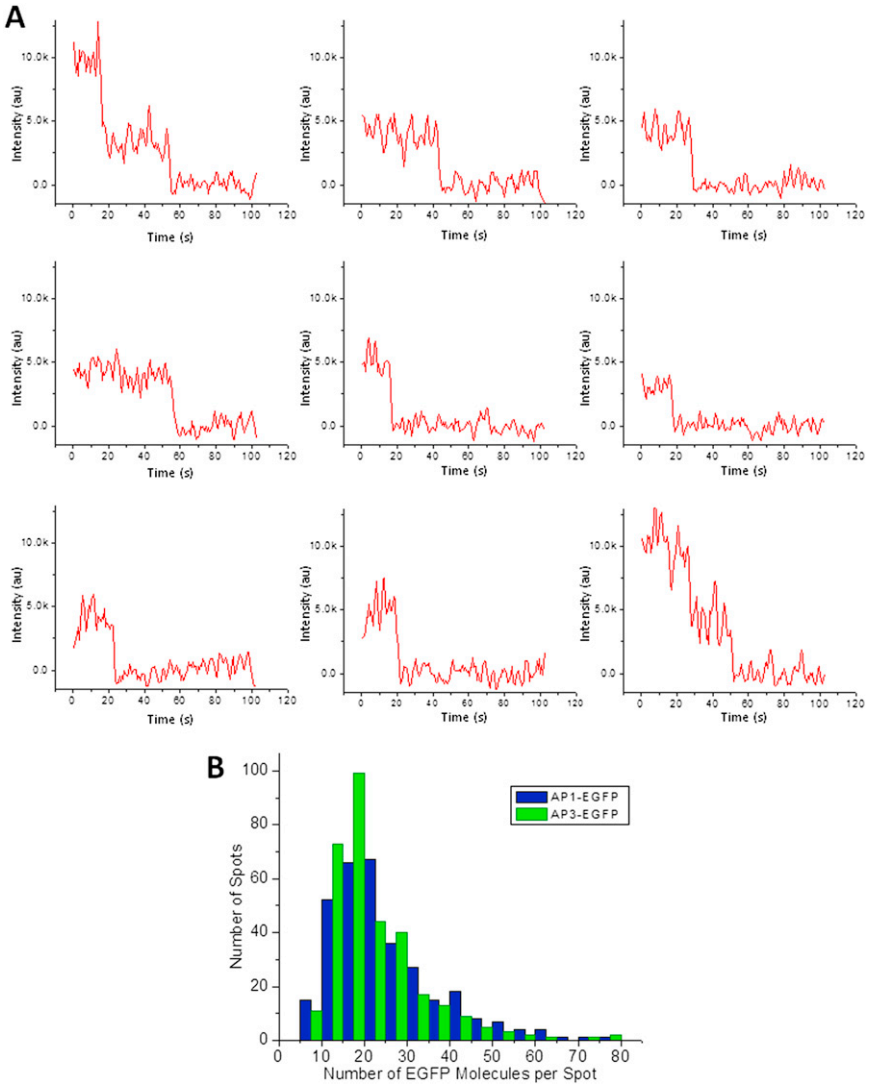

Figure S1. Number of AP1 and AP3 Adaptors Associated with Single Intracellular AP1- and AP-3-Containing Carriers, Related to Figure 1

(A) Single-molecule fluorescence intensity calibration using diluted cytosol purified from BSC1 cells stably expressing σ2-EGFP adsorbed to the glass coverslip. The tracings show representative examples of single photobleaching steps from isolated diffraction limited fluorescent spots of EGFP imaged using spinning disk confocal microscopy. Data are from a time-series acquired every 750 ms using 700 ms exposures. The fluorescence amplitude of the step was used to calibrate the fluorescence intensity associated with a single molecule of EGFP. The relative fluorescence intensity for a single EGFP molecule (4301 ± 1134; N = 94) followed the Gaussian distribution expected for single fluorophores (not shown).

(B) Histogram distribution of the number of AP1 and AP3 adaptors tagged with EGFP associated with single diffraction limited intracellular AP-containing carriers imaged in chemically fixed BSC1 cells stably expressing σ1-EGFP or σ3-EGFP, respectively. The fluorescence intensities were obtained from the maximum intensity projection extracted from a 3D stack of 15 optical sections spaced 200 nm, each obtained with 700 ms exposure. The number of EGFP molecules associated with a given AP1 (blue) or AP3 (green) spot was calculated by comparing their fluorescence intensity with the average relative fluorescence intensity of a single EGFP determined in (A) using the same imaging conditions. The number of σ1- or σ3-EGFP molecules associated with diffraction limited intracellular AP1- or AP3-containing carriers were 25 ± 13 (N = 325) and 22 ± 11 (N = 323), respectively.

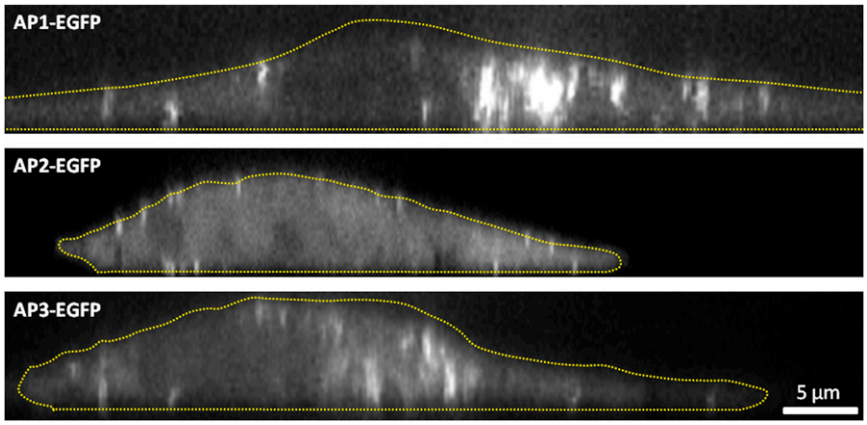

Figure S2. Cellular Distribution of AP1-, AP2-, and AP3-Containing Structures, Related to Figures 1, 2, and S3

3D live cell imaging of AP1-, AP2- or AP3-containing carriers in BSC-1 cells stably expressing σ1-EGFP, σ2-EGFP or σ3-EGFP, respectively. The representative views correspond to X-Z orthogonal projections of Z-stacks of 50 sequential optical sections spaced 100 nm each acquired with 100 ms exposure. Scale bar, 5 μm.

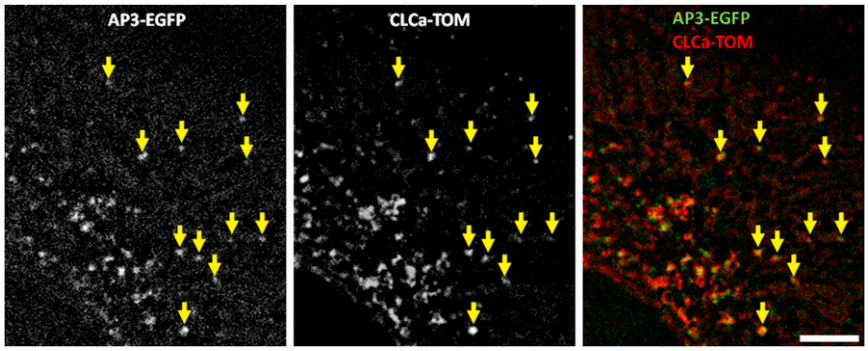

Figure S3. Extent of Colocalization of AP3 and Clathrin Determined by Live Cell Imaging, Related to Figures 2 and S4

The extent of colocalization of intracellular AP3 and clathrin was determined using spinning disk confocal microscopy of live BSC1 cells stably expressing σ3-EGFP (to label AP3) and transiently expressing clathrin light chain A–tomato (to label clathrin). Time-series from a single optical section were simultaneously acquired for both fluorophores from split images obtained every 1.5 s using a Dual View device placed in front of the camera with 25 ms exposures. The representative images from a single time point highlight the extensive colocalization of AP3 (left panel) with clathrin (center panel). Yellow arrows indicate a subset of objects containing AP3 and clathrin. While almost all AP3 spots colocalized with clathrin, only a fraction of clathrin colocalized with AP3; this is the expected result given that intracellular clathrin carriers containing AP3 do not contain AP1 or AP2. Scale bar, 5 μm.

Cell PRESS
Open ACCESS

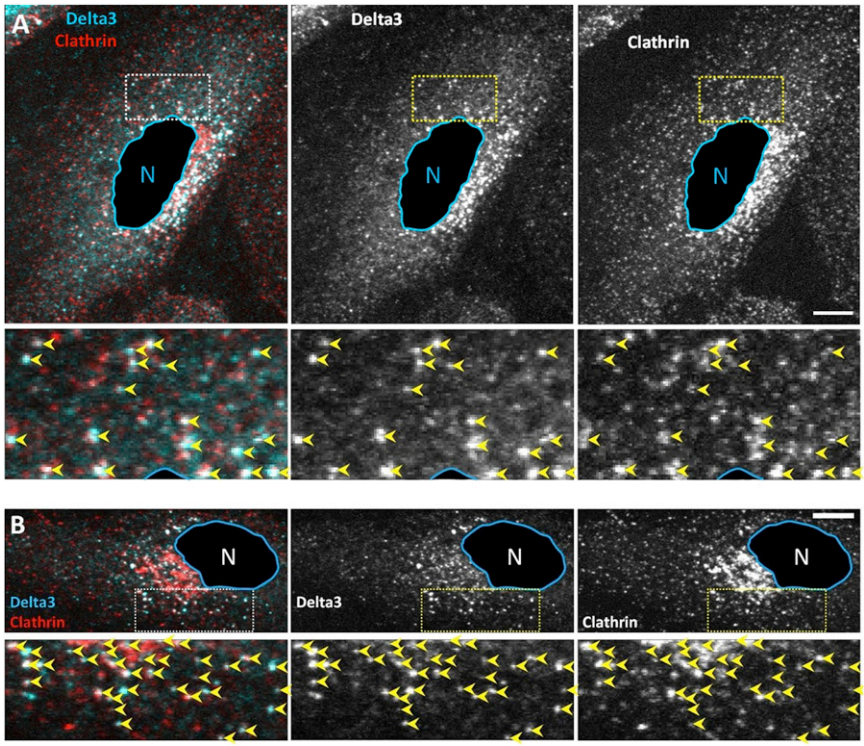

Figure S4. Extent of Colocalization of AP3 and Clathrin Determined by Immunofluorescence Microscopy, Related to Figures 1, 2, S3, and S4

BSC1 cells stably expressing σ3-EGFP (A) or σ2-EGFP (B) processed for immunofluorescence microscopy with antibodies specific for δ3-adaptin of AP3 (blue) and for clathrin light chain (red) were imaged in 3D by spinning disk confocal microscopy using optical sections spaced 0.25 μm. The representative images show a single optical section. Enlarged regions images of the boxed area are shown in the corresponding bottom panels where yellow arrowheads denote unambiguous instances of colocalization between AP3 and clathrin spots. Scale bars, 10 μm.